CARBON 50 (2012) 1488–1502

Available at www.sciencedirect.com

SciVerse ScienceDirect

journal homepage: www.elsevier.com/locate/carbon

Carbon molecular sieve dense film membranes derived from Matrimid® for ethylene/ethane separation

Meha Rungta, Liren Xu, William J. Koros *

Chemical & Biomolecular Engineering, Georgia Institute of Technology, 311 Ferst Drive, Atlanta, GA 30332-0100, USA

ARTICLE INFO

Article history:
Received 19 June 2011
Accepted 10 November 2011
Available online 19 November 2011

ABSTRACT

Development of dense film carbon molecular sieve (CMS) membranes for ethylene/ethane (C_2H_4/C_2H_6) separation is reported. A commercial polyimide, Matrimid®, was pyrolyzed under vacuum and inert argon atmosphere, and the resultant CMS films were characterized using pure C_2H_4 and C_2H_6 permeation at 35 °C, 50 psia feed pressure. The effects on C_2H_4/C_2H_6 separation caused by different final vacuum pyrolysis temperatures from 500 to 800 °C are reported. For all pyrolysis temperatures separation surpassed the estimated 'upper bound' solution processable polymer line for C_2H_4 permeability vs. C_2H_4/C_2H_6 selectivity. C_2H_4 permeability decreased and selectivity increased with increasing pyrolysis temperature until 650–675 °C where an optimum combination of C_2H_4 permeability ~14–15 Barrer with C_2H_4/C_2H_6 selectivity ~12 was observed. A modified heating rate protocol for 675 °C showed further increase in permeability with no selectivity loss. CMS films produced from argon pyrolysis showed results comparable to vacuum pyrolysis. Further, mixed gas (63.2 mol% C_2H_4 + 36.8 mol% C_2H_6) permeation showed a slightly lower C_2H_4 permeability with C_2H_4/C_2H_6 selectivity increase rather than a decrease that is often seen with polymers. The high selectivity of these membranes was shown to arise from a high 'entropic selection' indicating that the 'slimmer' ethylene molecule has significant advantage over ethane in passing through the rigid 'slit-shaped' CMS pore structure.

© 2011 Elsevier Ltd. All rights reserved.

1. Introduction

Ethylene, one of the largest volume organic chemicals, is an important precursor to polyethylene and organic chemicals such as ethylene dichloride and ethylene oxide.[1] The global ethylene production capacity in 2009 was 132.9 million tons per year (tpy), up nearly 5% from 126.7 million tpy in 2008 [1]. C_2H_4/C_2H_6 separation is carried out by cryogenic distillation (for e.g. −25 °C, 320 psig), an extremely energy intensive and expensive process because of the low relative volatility of C_2H_4 and C_2H_6 [2–5]. Potentially significant energy and cost savings make alternative C_2H_4/C_2H_6 separation technologies an important area of study.

Membrane technology provides an attractive alternative to cryogenic distillation because it potentially requires low energy and cost [6]. Currently dominant polymeric membranes are however limited by a trade-off between productivity (permeability) and efficiency (selectivity) [7–9]. They have shown relatively low C_2H_4/C_2H_6 selectivity (<7) with low C_2H_4 permeability (0.87–4.46 Barrers) in the upper selectivity range of 5–7 [10–13]. Facilitated transport membranes have shown promising C_2H_4/C_2H_6 separation, however, the intrinsic instability of these membranes makes them questionable for practical application [5,14–16].

Carbon molecular sieve (CMS) membranes, formed by high temperature pyrolysis of polymeric materials under controlled

* *Corresponding author:* Fax: +1 404 385 2683.
E-mail address: wjk@chbe.gatech.edu (W.J. Koros).

[1] http://www.dow.com/PublishedLiterature/dh_00bf/0901b803800bfd21.pdf?filepath=productsafety/pdfs/.

0008-6223/$ - see front matter © 2011 Elsevier Ltd. All rights reserved.
doi:10.1016/j.carbon.2011.11.019

conditions [17], are chemically inert and temperature resistant materials that have shown very promising separation performance exceeding the polymeric 'upper bound' for several gas separations [18–24].

Although more brittle compared to polymer membranes, CMS hollow fiber membranes have been shown to perform stably under high pressure natural gas feeds up to 1000 psi [25], and can avoid plasticization commonly encountered in polymeric membranes due to high pressure condensable feed gases [20,26,27].

C_2H_4/C_2H_6 separation using CMS membranes has been studied by few researchers [28–30], however low C_2H_4/C_2H_6 separation performance was reported. Fuertes and Menendez [30] prepared carbon membranes by carbonization (vacuum, 700 °C) of a thin phenolic resin film deposited on the inner surface of an alumina tube support. They studied the effect of pre-oxidation and post-oxidation in air on separation characteristics of their membranes. In some cases, their carbon membranes were modified by chemical vapor deposition (CVD) before or after air-oxidation. Their membranes showed C_2H_4/C_2H_6 selectivity in the range of 1.0–4.9 in all but one case. For one particular case where the membrane was subject to both post-oxidation at 350 °C and CVD modification, the selectivity was reported as 11 with C_2H_4 permeability ~4 Barrer (membrane thickness ~2 μm). Hayashi et al. [28] prepared membranes by carbonizing (inert argon stream, 700 °C) a BPDA-pp′ODA polyimide film formed on the outer surface of a porous alumina support. Their membranes show C_2H_4/C_2H_6 selectivity <6.9 in all cases. Okamoto et al. [29] prepared carbonized hollow fiber membranes by pre-oxidation and subsequent pyrolysis of asymmetric hollow fiber membrane of a BPDA-based polyimide at temperatures of 500–700 °C under nitrogen. These membranes were, however, primarily used for propane/propylene and 1,3-butadiene/*n*-butane separation and showed a low C_2H_4/C_2H_6selectivity of 3.1 with 600 °C pyrolysis.

Replacing C_2H_4/C_2H_6 distillation units with membrane separation may not yet be feasible due to the low C_2H_4/C_2H_6 selectivity or instability of current membrane materials. For example, for a realistic 62 mol% C_2H_4 + 38 mol% C_2H_6 feed, a membrane with a C_2H_4/C_2H_6 separation factor of 20 can only deliver a 97% C_2H_4 permeate, even under ideal conditions of downstream under vacuum and zero stage cut, and cannot achieve required purities >99 mol%. Nevertheless, with advanced C_2H_4/C_2H_6 separation membranes, a hybrid membrane-distillation system may still offer significant economic incentive and a practical approach to debottlenecking distillation units [3,4,31].

This paper addresses, in detail, the development of relatively high selectivity, free-standing CMS dense film membranes derived from the commercial polyimide Matrimid® and specially tailored for C_2H_4/C_2H_6 separation. We report a method for optimization of C_2H_4/C_2H_6 separation achieved by way of fine-tuning the pyrolysis conditions, with focus on the effects of different pyrolysis temperatures. This work thus intends to establish a basis for guiding research ultimately aimed at providing a convenient, potentially scalable hollow fiber membrane formation technology for C_2H_4/C_2H_6 separation.

2. Theory and background

2.1. Structure of CMS membranes

CMS membranes are formed by pyrolysis of polymer precursors under controlled conditions. The resulting 'turbostatic' structure comprises disordered, sp^2-hybridized, condensed hexagonal carbon sheets (Fig. 1a) with pores formed from packing imperfections [17,18,23,32,33]. An idealized 'slit-like' pore structure, as represented in Fig. 1b, can be described by a bimodal pore distribution (Fig. 1c), with larger pores (7–20 Å), called 'micropores', connected by smaller pore windows (<7 Å), called 'ultramicropores' [18]. This combination of micropores and ultramicropores provides both high flux and high efficiency via a molecular sieving function in CMS membranes.

2.2. Transport in CMS membranes

Gas transport in CMS membranes follows the sorption–diffusion model, wherein gas molecules sorb at the upstream face of the membrane, diffuse through the membrane under a chemical potential gradient, and desorb at the downstream side. Two key parameters define the separation performance of membrane materials: 'permeability', a measure of the membrane's intrinsic productivity, and 'selectivity', a measure of the membrane's separation efficiency.

Permeability is the pressure and thickness normalized flux, given as

$$P_A = \frac{n_A l}{\Delta p_A} \tag{1}$$

In Eq. (1) n_A represents the flux of component A through a membrane of thickness l and Δp_A is the partial pressure difference of A across the membrane. The unit for permeability is Barrer, where,

$$1\ \text{Barrer} = 10^{-10}\frac{\text{cc(STP)}\cdot\text{cm}}{\text{cm}^2\cdot\text{s}\cdot\text{cmHg}} \tag{2}$$

Another popular unit for permeability is $\frac{\text{kmol}}{\text{m}^2\cdot\text{s}\cdot\text{kPa}}$ ($1\ \text{Barrer}\times 2.99\times 10^{15} = 1\,\frac{\text{kmol}\cdot\text{m}}{\text{m}^2\cdot\text{s}\cdot\text{kPa}}$). Permeability can also be represented as the product of a kinetic factor, i.e. the diffusion coefficient, D_A, and a thermodynamic factor, i.e. the sorption coefficient $\mathbb{S}_A$:

$$P_A = D_A\mathbb{S}_A \tag{3}$$

The molecular sieving ultramicropores can effectively separate similar sized gas molecules because even small changes in size can result in considerable differences in the activation energy required to make a diffusive jump, referred to as 'energetic selectivity'. In addition, unlike conventional polymers, CMS membranes can provide high 'entropic selectivity' since the rigid ultramicropore windows can effectively restrict the degrees of freedom of rotation and internal vibration of the rejected molecule [24,34,35].

The sorption coefficient, $\mathbb{S}_A$, equals the ratio of the sorbed gas concentration, C_A, and the partial pressure, p_A. It depends on the condensability of the gas penetrant and its interactions with the membrane material. For CMS membranes micropores provide the majority of the sorption volume,

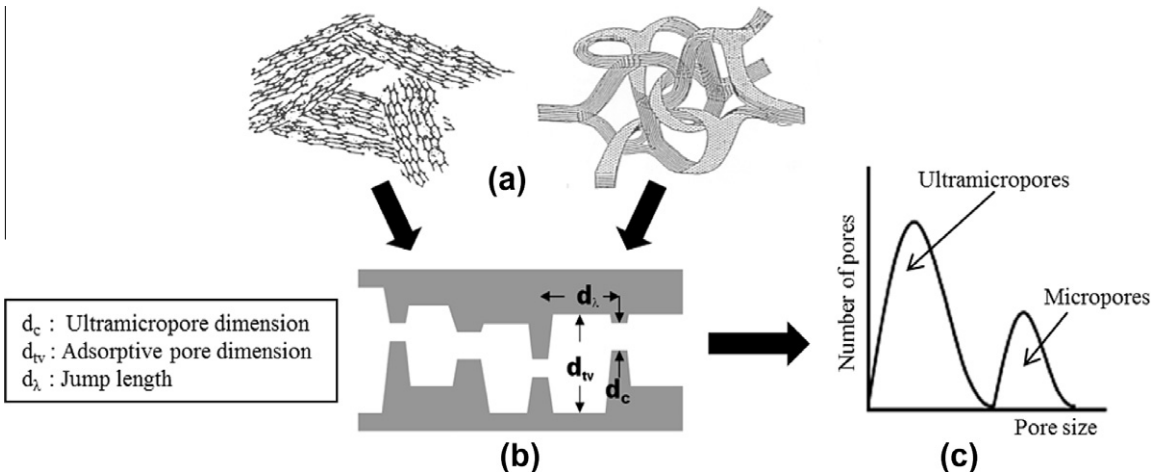

Fig. 1 – (a) Structure of pyrolytic carbon [32,33], (b) idealized pore structure of CMS membrane [18], (c) idealized bimodal pore size distribution of CMS membrane [18].

and the sorption coefficient is defined as the secant slope of the applicable Langmuir isotherm, viz.

$$\mathbb{S}_A = \frac{C_A}{p_A} = \frac{C'_{HA} b_A}{1 + b_A p_A} \tag{4}$$

where C'_{HA} is the Langmuir hole-filling capacity and b_A is Langmuir affinity constant.

The separation factor is defined as the ratio of the permeate-side and feed-side mole fractions y and x, respectively of the two components A and B. When the downstream pressure is negligible compared to the upstream pressure, as in the current study, the selectivity is equal to the ratio of the component permeabilities. Thus,

$$\alpha_{A/B} = \frac{(y_A/y_B)_{\text{permeate}}}{(x_A/x_B)_{\text{feed}}} = \frac{P_A}{P_B} = \frac{D_A}{D_B}\frac{\mathbb{S}_A}{\mathbb{S}_A} \tag{5}$$

For C_2H_4/C_2H_6 separation, because of the similar condensability and critical temperature of the two penetrants, high diffusion selectivity may be required to provide a useful selectivity in Eq. (5). In this regard, 'entropic selectivity', which is lacking in polymeric membranes, may be a key feature enabling CMS membranes for the C_2H_4/C_2H_6 pair.

2.3. *Temperature dependence of permeation, diffusion and sorption*

Permeability of a penetrant through a membrane material, polymer or molecular sieving, follows Arrhenius-type temperature dependence.

$$P = P_o \exp\left(\frac{-E_P}{RT}\right) \tag{6}$$

where P_o is the pre-exponential factor, E_P is the apparent activation energy for permeation of a penetrant through a given material, R is the universal gas constant and T is the absolute temperature.

Diffusion in CMS membranes is an activated process and increases with temperature according to the Arrhenius relationship (Eq. (7)). The thermodynamic sorption coefficient decreases with temperature following van't-Hoff equation (Eq. (8)).

$$D = D_o \exp\left(\frac{-E_D}{RT}\right) \tag{7}$$

$$\mathbb{S} = \mathbb{S}_o \exp\left(\frac{-H_{\mathbb{S}}}{RT}\right) \tag{8}$$

where D_o and $\mathbb{S}_o$ are pre-exponential factors for diffusion and sorption respectively, E_D is the apparent activation energy for diffusion and $H_{\mathbb{S}}$ is the apparent heat of sorption.

From Eqs. (3) and (6)–(8), we get

$$P = P_o \exp\left(\frac{-E_P}{RT}\right) = D\mathbb{S} = D_o \exp\left(\frac{-E_D}{RT}\right)\mathbb{S}_o \exp\left(\frac{-H_{\mathbb{S}}}{RT}\right) \tag{9}$$

which gives

$$P_o = D_o \mathbb{S}_o \tag{10}$$

$$E_P = E_D + H_{\mathbb{S}} \tag{11}$$

The temperature dependence of permeability is less pronounced than that of diffusion, i.e. the activation energy for permeation is not as high as diffusion, which is primarily due to typical negative heats of sorption. The increase in diffusivity however outweighs the decrease in sorption coefficient resulting in an increase in permeability with temperature. Selectivity, on the other hand, is generally found to decrease slightly with temperature since an increase in temperature in most cases results in a greater increase in permeability of the larger penetrant molecule. When 'entropic selectivity' dominates the diffusion selectivity, however, this undesirable trade-off may be avoided.

2.4. *Energetic and entropic contributions to diffusion selectivity*

Diffusion in CMS increases with temperature according to Arrhenius relationship (Eq. (7)). The pre-exponential factor D_o can be represented from transition state theory as

$$D_o = e\lambda^2 \frac{kT}{h} \exp\left(\frac{S_D}{R}\right) \tag{12}$$

where λ is the average diffusive jump length, S_D is the activation entropy of diffusion, k is Boltzmann's constant, and h is

Planck's constant [35,36]. Note that the S used for entropy is different from the $\mathbb{S}$ used for the sorption coefficient. For a gas pair 'A' and 'B' of similar size λ can be considered equal for both molecules [34,35,37]. The diffusion selectivity is thus obtained from Eqs. (7) and (12) as

$$\frac{D_A}{D_B} = \frac{D_{Ao}}{D_{Bo}} \exp\left(-\frac{E_{D_A} - E_{D_B}}{RT}\right) = \underbrace{\exp\left(\frac{S_{D_A} - S_{D_B}}{R}\right)}_{\text{Entropic selectivity}} \underbrace{\exp\left(-\frac{E_{D_A} - E_{D_B}}{RT}\right)}_{\text{Energetic selectivity}} = \exp\left(\frac{\Delta S_{D_{A,B}}}{R}\right) \exp\left(-\frac{E_{D_{A,B}}}{RT}\right) \quad (13)$$

From the transition state theory, the diffusion coefficient can also be described as

$$D = \lambda^2 \frac{kT}{h} \frac{F^{\neq}}{F} \exp\left(\frac{-E_D}{RT}\right) \quad (14)$$

where $F = F_{trans} \cdot F_{rot} \cdot F_{vib}$ is the partition function of a gas molecule in the normal state and $F^{\neq}$ is its partition function in the transition state [34,38]. In the normal state, the gas molecule sits in a micropore and the transition state occurs as it passes through the ultramicropore window [34]. $F^{\neq}$ does not contain the translational degree of freedom in the direction of diffusion and this is accounted for by the factor kT/h [34]. Combining Eqs. (12)–(14) we get the 'entropic selectivity' as

$$\exp\left(\frac{\Delta S_{D_{A,B}}}{R}\right) = \frac{(F^{\neq}/F)_A}{(F^{\neq}/F)_B} = \frac{D_{Ao}}{D_{Bo}} \quad (15)$$

The ultramicropores in CMS membranes, which are analogous to the selective window opening in zeolites, can restrict the rotational and internal vibrational degrees of freedom of one molecule compared to the other. This capability can be especially useful for similar sized molecules like C_2H_4 and C_2H_6.

2.5. *Factors affecting transport through CMS membranes*

The separation performance of CMS membrane can be controlled by optimally tuning its critical pore size and pore size distribution depending on the relative sizes of the gas pair being separated. The key tuning parameters include (1) polymer precursor material, (2) pre-treatment conditions, (3) pyrolysis conditions, i.e. the heating protocol (final pyrolysis temperature, ramp rates and soak times) and the pyrolysis atmosphere (vacuum, inert gas, presence of oxygen, etc.) and (4) post-treatment conditions. The effects of these factors on CMS performance for a variety of gas pairs has been investigated by several researchers [20–23,39–44]. However, to date, a stable, reproducible CMS membrane prepared readily from a commercially available material and offering improved performance in C_2H_4/C_2H_6 separation has not been demonstrated.

3. Experimental

3.1. *Polymer precursor dense film formation*

Commercially available polyimide Matrimid® 5218 obtained from Huntsman International LLC in the form of powder was used in the work. The polymer powder was first dried in a vacuum oven at 120 °C for at least 12 h to remove moisture. The dried powder was dissolved in dichloromethane (⩾99.8% purity, Sigma–Aldrich) to form a 3–5 wt% polymer solution and placed on a roller for at least 6 h for mixing. The polymer solution was used to prepare polymer dense films by a solution casting method in a glove bag at room temperature to achieve slow evaporation rate (3–4 days) and the vitrified films were then removed and dried in a vacuum oven at 120 °C for at least 12 h to remove residual solvent. The dried films were then cut using a die-cutter into 2.22 cm circles for pyrolysis. All films had a thickness of 70 ± 10 μm for consistency.

3.2. *CMS dense film formation*

The polymer films cut into small circles were placed on a channeled quartz plate (United Silica Products, Franklin, NJ), which allowed for diffusion of the volatile by-products evolved from pyrolysis. This was then loaded into a quartz tube (National Scientific Company, GE Type 214 quartz tubing, Quakertown, PA) and placed in the pyrolysis setup shown in Fig. 2.

The pyrolysis setup was similar to previous reported apparatus [19,25], with some modifications. It consists of a three-zone furnace (Thermcraft, Inc., model XST-3-0-24-3C, Winston-Salem, NC) with three thermocouples connected independently to three channels of a multi-channel temperature controller (Omega Engineering, Inc., model CN1504TC, Stamford, CT), thus allowing accurate and uniform control of the temperature profile inside the quartz tube. The quartz tube was sealed on either side using an assembly of metal flanges with silicon O-rings (MTI Corporation, Richmond, CA). The set-up was equipped to perform pyrolysis under vacuum, monitored using a 0–1000 mtorr pressure transducer (MKS, model 628 Absolute Capacitance Manometer, Andover, MA), or purge gas atmosphere. An oxygen analyzer (Cambridge Sensotec Ltd., Rapidox 2100 series, Cambridge, England) was integrated into the set-up to monitor the concentration of oxygen present during pyrolysis.

Matrimid® dense film pyrolysis was performed under vacuum (⩽10 mtorr) for a range of temperatures between 500 and 800 °C, specifically at 500, 525, 550, 650, 675 and 800 °C, using the heating protocols (Fig. 3a) listed below.

Protocol 1: For final temperatures up to 550 °C:

(1) 50 → 250 °C at a ramp rate of 13.3 °C/min.
(2) 250 °C → (T_{max} −15)°C at a ramp rate of 3.85 °C/min.
(3) (T_{max} −15)°C → T_{max} °C at a ramp rate of 0.25 °C/min.
(4) Soak for 2 h at T_{max}.

Protocol 2: For final temperatures above 550 up to 800 °C:

(1) 50 → 250 °C at a ramp rate of 13.3 °C/min.
(2) 250 → 535 °C at a ramp rate of 3.85 °C/min.
(3) 535 → 550 °C at a ramp rate of 0.25 °C/min.
(4) 550 → (T_{max} −15)°C at a ramp rate of 3.85 °C/min.
(5) (T_{max} −15)°C → T_{max} °C at a ramp rate of 0.25 °C/min.
(6) Soak for 2 h at T_{max}.

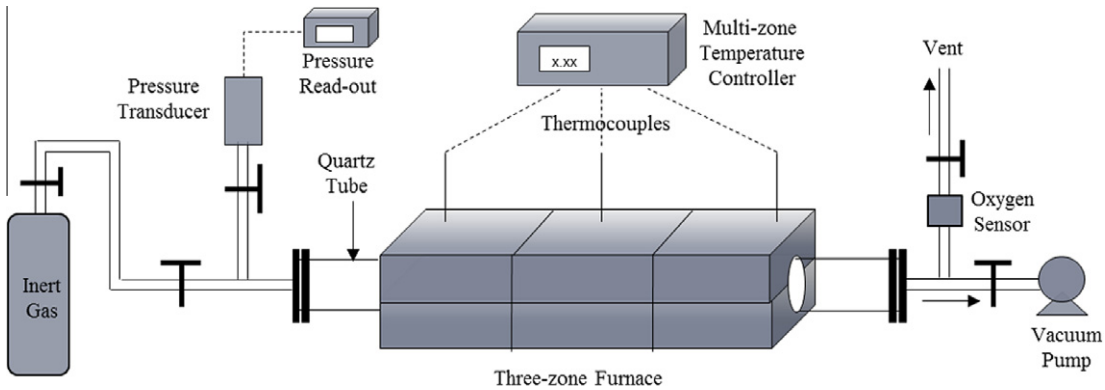

Fig. 2 – Pyrolysis set-up.

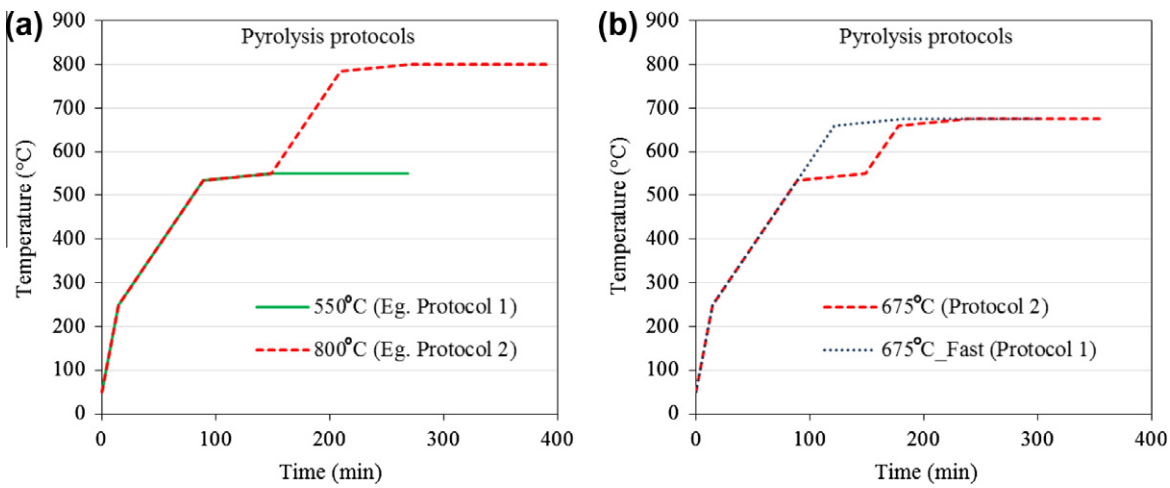

Fig. 3 – Pyrolysis heating protocols (a) 550 °C protocol shown as an example for Protocol 1 (green) for temperatures up to 550 and 800 °C protocol shown as an example for Protocol 2 (red) for temperatures above 550 °C and up to 800 °C, (b) 675 °C Protocol 2 (red) and 675 °C_Fast protocol (black) similar to Protocol 1 but ends at 675 °C. (For interpretation of the references to color in this figure legend, the reader is referred to the web version of this article.)

Unless otherwise specified, all films were pyrolyzed using the applicable heating protocol (either Protocol 1 for temperatures up to 550 °C or Protocol 2 for temperatures above 550 °C) as stated above. The films were named based on the final pyrolysis temperature as 500 °C-CMS, 525 °C-CMS, 550 °C-CMS and so on.

After the heating cycle was complete, the furnace was allowed to cool down naturally, while remaining under vacuum or inert gas flow, to below 50 °C before venting the furnace and unloading the samples. All samples were stored under vacuum before and after permeation measurements to eliminate changes in CMS performance due to atmospheric exposure prior to testing.

After each pyrolysis run, both the quartz tube and the channeled quartz plate were thoroughly cleaned with acetone and baked in air at 800 °C for 2 h to clean out any residue and to prevent contamination in the subsequent run.

In addition to the pyrolysis protocols listed above, a film was also pyrolyzed at a final pyrolysis temperature of 675 °C using Protocol 1 instead of (the slow step process in) Protocol 2 (see Fig. 3b). This film was named 675 °C_Fast-CMS, because the modified protocol for this film used a shorter (faster) ramp time compared to the traditional Protocol 2 for temperatures over 550 °C.

Inert gas pyrolysis was also performed at 550 and 675 °C using Protocol 1 following the same procedure listed above but instead of pulling vacuum, a controlled flow of argon (Ultra High Purity, Airgas) was used during pyrolysis.

3.3. *Dense film permeation measurement*

Precursor and CMS dense films were masked and loaded into permeation cells. Details of masking and preparation of permeation cell have been described in previously [19]. The permeation cell was then placed in a constant-volume permeation system [45,46]. The entire system (upstream and downstream) was evacuated for at least 24 h and a leak rate was measured (<1% of the permeation rate of the slowest gas). After leak test and evacuation, the upstream was pressurized with feed gas (50 psia ~3.4 atm) while the downstream was kept at vacuum. The system temperature was kept at 35 °C. The pressure rise in a constant downstream volume was recorded over time using LabVIEW (National

Instruments, Austin, TX) until steady state was achieved and permeability was calculated using Eq. (1). The system was evacuated before each experiment for 10 times the time lag of the previous gas tested.

The permeation raw data was used to estimate the apparent diffusivity (D) from the time-lag method (Fig. 4) as follows:

$$D = \frac{l^2}{6\theta} \tag{16}$$

where θ is the observed permeation time-lag and l is the film thickness. This was further used to calculate the apparent sorption coefficient ($\mathbb{S}$) from Eq. (3) and the respective diffusion and sorption selectivities.

3.4. *Thermo gravimetric analysis (TGA)*

TGA (Netzsch, STA 409 PC Luxx TGA.DSC) was performed to analyze the percentage mass loss due to pyrolysis. Prior to start, all samples were purged with helium (UHP, Air Gas) for at least 6 h and measurements were carried out under 30 cc/min helium with the same heating protocols used for pyrolysis.

4. Results and discussion

4.1. *Estimated experimental upper-bound for ethylene/ethane separation*

Solution processable materials appropriate for forming high flux asymmetric hollow fiber membranes for gas separation are limited by a trade-off between the selectivity for the gas pair and the fast gas permeability, commonly referred to as the 'upper bound'. In 1991, Robeson published the polymeric upper-bound trade-off curves for several light gas pair separations including O_2/N_2, H_2/CH_4, CO_2/CH_4, He/O_2 and other combinations involving these gas molecules [7]. Since then, continuous efforts to improve gas transport properties of hyper-rigid glassy polymers by tailoring their structure and perfluorinated polymers have successfully shifted the upper bound [8]. In 2003, based on a review of available data, Burns and Koros estimated the upper bound for C_3H_6/C_3H_8 separation [9]. Given the limited research conducted in the field of C_2H_4/C_2H_6 separation, no comprehensive upper-bound compilation is available yet. In order to compare CMS membrane performance with existing polymer membrane materials, we have used available literature data [10–13] and measurements made in this work to estimate the upper-bound for the C_2H_4/C_2H_6 gas pair, as shown in Table 1 and Fig. 5.

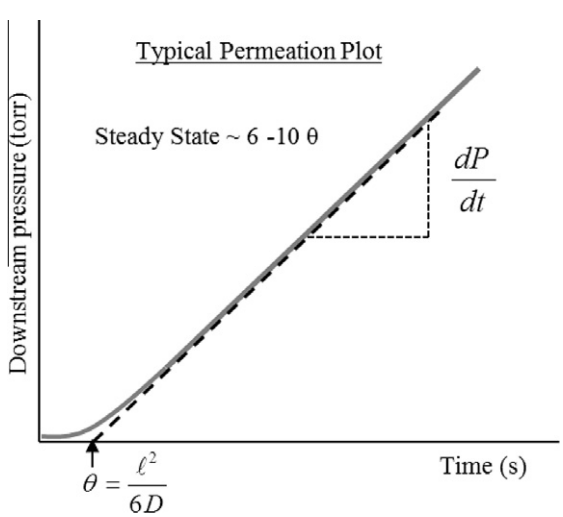

Fig. 4 – Calculation of apparent diffusivity (D) from permeation time-lag (θ).

Measurements reported herein are based on pure gas steady state permeation tests at 35–50 °C and 2–5 atm feed pressure. As noted in the references [10–13] adopted for the upper bound estimation, plasticization effects in these materials due to C_2H_4 and C_2H_6 are shown to be non-existent in this pressure range. A 1992 publication by Ilinitch et al. [47] reports C_2H_4 and C_2H_6 permeability and C_2H_4/C_2H_6 selectivity from a gas mixture containing 85 vol% CH_4, 10 vol% C_2H_4 and 5 vol% C_2H_6 for polyphenyleneoxide (PPO), two PPO-based copolymers and several rubbery polymers. In a 1993 article the same authors [48] published a corrigendum stating that due to a technical error, the permeabilities reported in 1992 [47] were one order of magnitude higher than the actual values. The results obtained by Ilinitch et al. [47,48] have not been included in predicting the upper bound since the authors express that these results were obtained from transient state permeation experiments. It should be noted that the experimental upper bound constructed here is based on high performing 6FDA-based polyimides which are the current best class of polymeric materials for gas separations, and can hence be considered a good estimate of the trade-off curve for C_2H_4/C_2H_6 separation.

4.2. *Preliminary study*

The intrinsic polymer precursor properties can significantly affect the final CMS membrane. Thus, selecting an appropriate polymer precursor is important. To date, few polymers have been pyrolyzed and used for C_2H_4/C_2H_6 separation. These include a phenolic-resin-based and BPDA-based polymer [28–30]. It is thus useful to determine the viability of C_2H_4/C_2H_6 separation using CMS dense films prepared from Matrimid® as the precursor material. CMS dense films were obtained by pyrolyzing Matrimid® precursor films under vacuum ($\leqslant$10 mtorr) at 550 and 800 °C using Protocol 1 and Protocol 2, respectively as listed earlier. The CMS dense films obtained were tested for pure gas C_2H_4 and C_2H_6 permeation at 35 °C and 50 psia feed pressure. In addition, a Matrimid® precursor dense film was also tested for pure gas C_2H_4 and C_2H_6 permeation at 35 °C and 50 psia feed pressure. The results for both the precursor and the CMS dense films were plotted against the experimental upper bound as shown in Fig. 6.

Clearly, Matrimid® CMS dense films can surpass the upper bound for C_2H_4/C_2H_6 separation for both the 550 °C-CMS and the 800 °C-CMS. The C_2H_4permeability for the 550 °C-CMS represents >3000% increase from the precursor permeability; however the selectivity is only slightly higher (<50% increase from the precursor selectivity). Steel and Koros [18] reported a high CO_2/CH_4 selectivity of 65 for Matrimid® pyrolyzed under vacuum at 550 °C (Protocol 1), which represents ~100%

Table 1 – Pure gas C_2H_4 permeability and C_2H_4/C_2H_6 selectivity data for different polymeric materials.

Precursor	T (°C)	p (atm)	$P_{C_2H_4}$ (Barrer)	$\alpha_{C_2H_4/C_2H_6}$	Source
6FDA–6FpDA	35	5.0	1.90	4.20	[10]
6FDA–1,5-NDA	35	5.0	0.87	5.80	
6FDA–NDA	35	2.0	1.17	6.84	[11]
6FDA–NDA/Durene (75:25)	35	2.0	4.46	5.62	
6FDA–NDA/Durene (50:50)	35	2.0	9.48	4.27	
6FDA–NDA/Durene (25:75)	35	2.0	36.70	3.60	
6FDA–Durene	35	2.0	76.70	2.89	
6FDA–TrMPD	50	2.0	58.00	2.90	[12]
BPDA–TeMPD	50	2.0	5.80	4.30	
6FDA–mPD	35	3.8	0.30	3.30	[13]
6FDA–IPDA	35	3.8	1.40	3.80	
6FDA–6FpDA	35	3.8	2.10	4.40	
Matrimid®	35	3.4	0.45	4.50	This work
6FDA–DAM	35	3.4	64.00	3.00	This work
6FDA:BPDA–DAM	35	3.4	46.00	3.30	This work

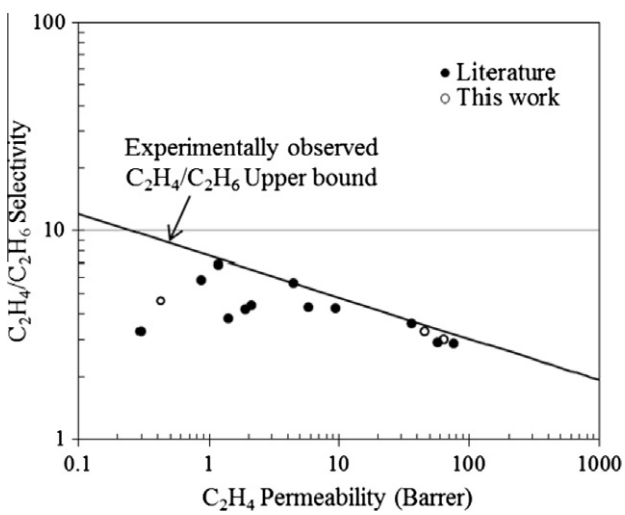

Fig. 5 – Experimental C_2H_4/C_2H_6 polymeric upper bound estimated using available polymeric pure gas C_2H_4 permeability and C_2H_4/C_2H_6 selectivity data, with line drawn to aid the eye. See Table 1.

increase from the precursor selectivity reported in their study. At 550 °C, however, the C_2H_4/C_2H_6 selectivity obtained in our study is not significantly higher compared to the starting polymer, nor is it much higher than that reported by previous researchers [28–30]. The Matrimid® 800 °C-CMS, on the other hand, can give C_2H_4/C_2H_6 selectivity as high as 12, >160% increase from the precursor material. However, while Steel and Koros [18] reported a CO_2 permeability of 66 Barrers, which is by no means low, with an exceptionally high CO_2/CH_4 selectivity of 209 for Matrimid® pyrolyzed at 800 °C under vacuum, our C_2H_4 permeability is low (<0.2 Barrer) which would present problems for commercial applications. It is thus desired to optimize the pyrolysis conditions, and to understand the resulting effects, for Matrimid® to obtain CMS dense films with both good C_2H_4 permeability as well as high C_2H_4/C_2H_6 selectivity.

4.3. *Effect of pyrolysis temperature on ethylene/ethane separation performance*

In order to study the effect of pyrolysis temperature on C_2H_4/C_2H_6 separation performance, Matrimid® dense films were pyrolyzed under vacuum (⩽10 mtorr) for a range of temperatures between 500 and 800 °C, specifically at 500, 525, 550, 650, 675 and 800 °C using the applicable pyrolysis protocol (Protocol 1 or Protocol 2) listed above. The CMS dense films obtained were tested for pure gas C_2H_4 and C_2H_6 permeation at 35 °C and 50 psia feed pressure. The C_2H_4 permeability and C_2H_4/C_2H_6 selectivity results are shown in Fig. 6. As seen from Fig. 6, for each of the pyrolysis temperatures, performance (either permeability or selectivity or both) of the CMS membranes is significantly better than that of the precursor and surpasses the estimated polymeric upper bound for C_2H_4/C_2H_6 separation. The C_2H_4 permeability and C_2H_4/C_2H_6 selectivity was plotted against the final pyrolysis temperature as shown in Fig. 7. It is seen that as pyrolysis temperature increases, permeability drops drastically up to 550 °C with a corresponding increase in selectivity. From 550 up to 675 °C, selectivity continues to increase significantly with a very small loss in permeability. Beyond 675 °C, permeability drops drastically again but without significant increase in selectivity. The optimum C_2H_4/C_2H_6 separation performance appears to lie in the range of 650–675 °C.

The diffusion and sorption coefficients as well as the respective selectivities were calculated using the time-lag method described above. As seen from Fig. 8, the C_2H_4 diffusion coefficient follows a similar trend as its permeability, decreasing with increase in pyrolysis temperature thus reflecting as a decrease in permeability. The sorption coefficient does not seem to follow any particular trend and direct sorption experiments are required to understand this further by detailed analysis of isotherms. The diffusion selectivity increases with pyrolysis temperature from 3 to 7 (Fig. 8) and remains fairly constant thereafter, following a trend similar to the overall selectivity. The sorption selectivity (plotted on the same scale as diffusion selectivity) remains in the range of 1.1–1.8 (Fig. 9) and, relative to diffusion selectivity, changes

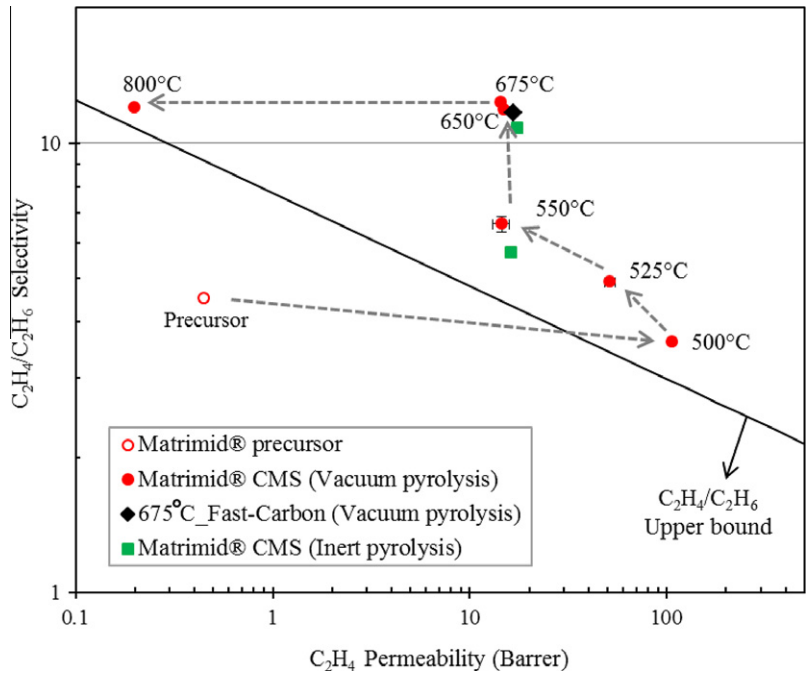

Fig. 6 – Comparison of Matrimid® CMS dense film C_2H_4/C_2H_6 separation performance vs. Matrimid® precursor separation (open red circles). Vacuum pyrolyzed CMS films are shown as closed red circles and inert pyrolyzed CMS are shown as green squares. The black diamond represents the 675 °C_Fast-CMS pyrolyzed under vacuum. The estimated experimental C_2H_4/C_2H_6 polymeric upper bound line is shown. Performance of CMS membranes exceeds the upper bound line. The data points at 525, 650 and 675 °C represent an average over two CMS films each while the 550 °C is an average of three CMS films (error bars are shown). In all cases checked, the reproducibility was good (with standard deviations <10% in permeability and <5% in selectivity). Inert pyrolysis at 550 and 675 °C using Protocol 1 shows results similar to vacuum pyrolysis. (For interpretation of the references to color in this figure legend, the reader is referred to the web version of this article.)

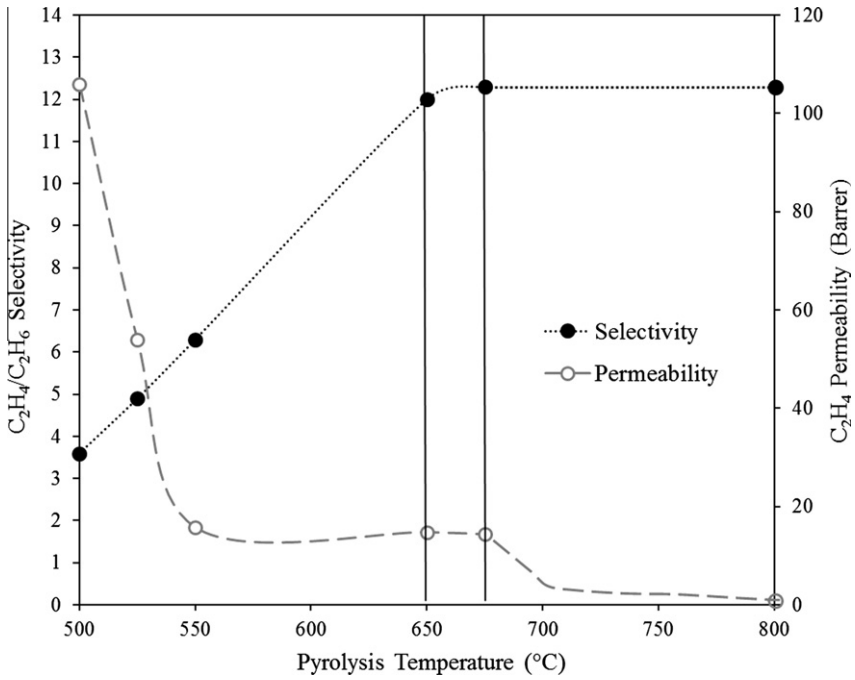

Fig. 7 – Effect of pyrolysis temperature on C_2H_4 permeability and overall C_2H_4/C_2H_6 selectivity of Matrimid® derived CMS dense film membranes.

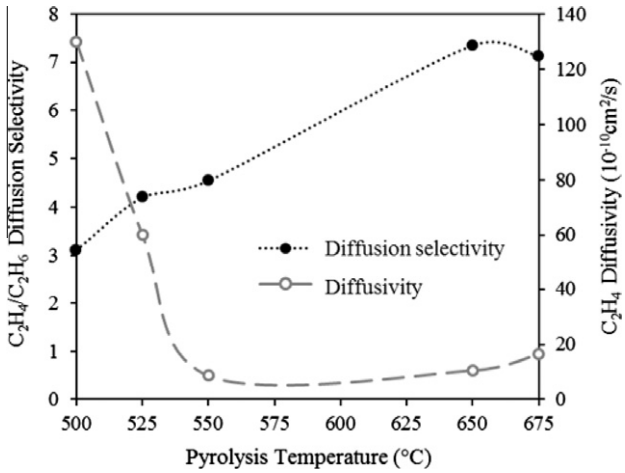

Fig. 8 – Effect of pyrolysis temperature on C_2H_4 diffusivity and C_2H_4/C_2H_6 diffusion selectivity of Matrimid® derived CMS dense film membranes. Diffusivity and diffusion selectivity are calculated using the permeation time-lag data as described. The C_2H_4 diffusivity for the 800 °C-CMS is $\sim 6 \times 10^{-11}$ cm²/s. The C_2H_6 diffusivity is on the order of 10^{-12} cm²/s and could not be computed accurately because of the unusually long time lag (>12 days to reach steady state). The 800 °C point has thus been excluded.

little (~50% change in sorption selectivity as opposed to a change in diffusion selectivity ~140–150%) with the pyrolysis temperature despite overall selectivity changes.

These effects can be explained qualitatively by considering the changes in the hypothetical, semi-quantitative ultramicropore size distribution (Fig. 10) proposed by Steel and Koros [39,40]. In Fig. 10, penetrant molecules are represented according to size along the abscissa, thereby providing an effective semi-quantitative molecular scale ruler. A given penetrant has free diffusive access to all inter-connected pores to the right of the line drawn at its characteristic size. Further, the

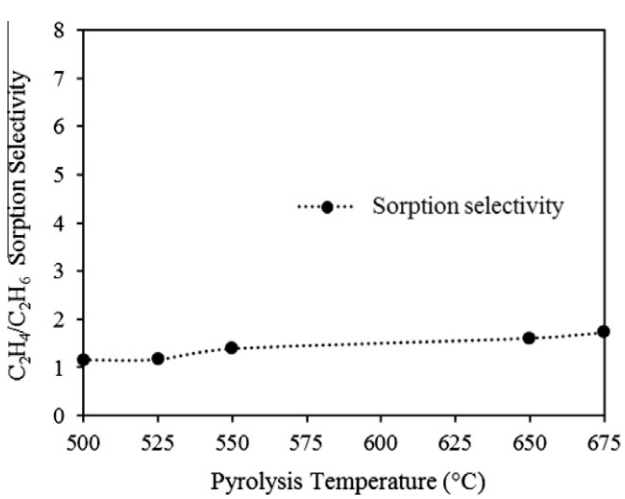

Fig. 9 – Effect of pyrolysis temperature on C_2H_4/C_2H_6 sorption selectivity of Matrimid® derived CMS dense film membranes. The 800 C point has been excluded for the same reason stated above in Fig. 8.

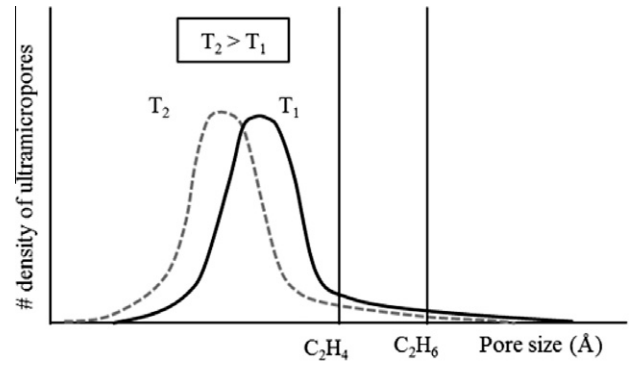

Fig. 10 – Hypothetical ultramicropore distributions. The solid black curve shows the hypothetical ultramicropore diffusion that may result at a final pyrolysis temperature T_1. When the final pyrolysis temperature is increased to T_2, the hypothetical ultramicropore distribution shifts to a smaller average pore size, represented by the dashed grey curve.

ratio of the areas under the curve to the right of the respective line for each penetrant represents the selectivity. With increase in the final pyrolysis temperature, the critical molecular sieving ultramicropore distribution shifts to a smaller average pore size resulting in a decrease in diffusivity, and hence permeability, for both C_2H_4 and C_2H_6, but the pores also become more selective as a relatively larger number of pores still remain accessible to the "skinnier" molecule C_2H_4 but not to C_2H_6. There is however a limit to such increase in selectivity with pyrolysis temperature, as for the 800 °C-CMS, when most of the pores become blocked to both C_2H_4 and C_2H_6 resulting in a drastic loss in permeability with no significant increase in the selectivity.

4.4. *Further optimization of ethylene/ethane separation performance*

A modified temperature protocol was used wherein a Matrimid® precursor film was pyrolyzed at a final pyrolysis temperature of 675 °C using Protocol 1, instead of going through the traditional slow step process in Protocol 2 for temperatures over 550 °C (see Fig. 3b). This modified pyrolysis protocol resulted in a small increase in permeability without loss in selectivity, yielding very attractive separation performance with a C_2H_4 permeability of ~17 Barrers and a high C_2H_4/C_2H_6 selectivity of ~12. As seen from the TGA curves shown in Fig. 11, the 675 °C_Fast-CMS shows a slightly larger mass loss compared to the 675 °C-CMS. These results compare well with mass loss data collected during the actual pyrolysis process under vacuum for the 675 °C protocol and 675 °C_Fast protocol as is shown in Table 2. For the 675 °C_Fast-CMS, rapid mass loss starts around 480 °C, the decomposition temperature for Matrimid®, and continues until 660 °C due to evolution of pyrolysis by-products. After 660 °C, densification of the carbon matrix takes place with a very small mass loss. For the 675 °C-CMS instead, rapid mass loss takes place only from 480 °C to about 550 °C after which the rate of evolution of pyrolysis by-products slows down before densification starts to occur, resulting in a smaller overall mass loss with greater shrinkage of CMS pores. Evolution of pyrolysis

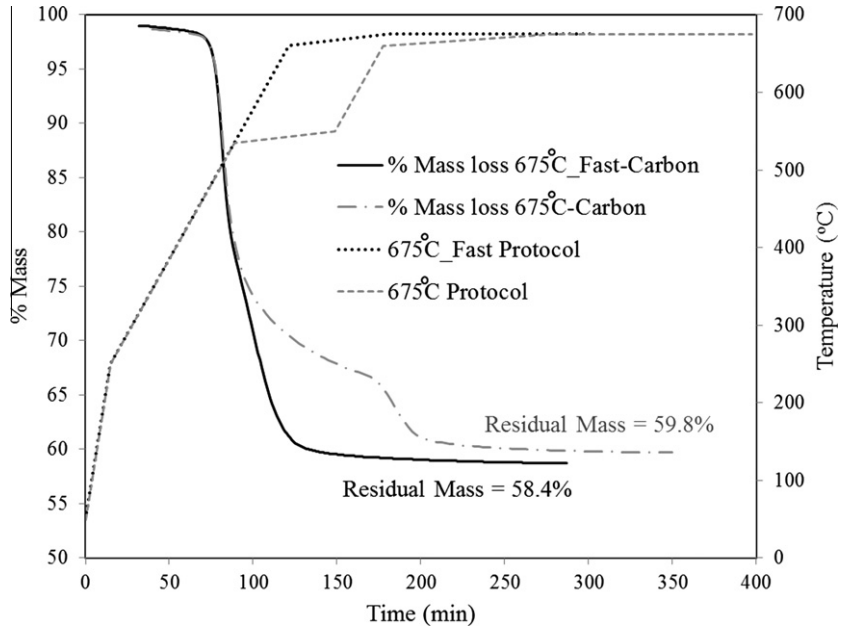

Fig. 11 – TGA mass loss curve for 675 °C_Fast-CMS and 675 °C-CMS.

by-products is believed to contribute to the CMS pore structure and sintering of the defects lead to ultramicropore tuning. It appears reasonable, therefore, that the 675 °C_Fast carbon shows slightly higher permeability compared to the 675 °C-CMS, while retaining the high selectivity. This is also reflected in the slight increase in both the diffusion and sorption coefficients for the 675 °C_Fast-CMS.

4.5. *Effect of pyrolysis atmosphere on ethylene/ethane separation performance*

Matrimid® precursor dense films were pyrolyzed at 550 and 675 °C using Protocol 1 as described above except that instead of drawing vacuum a controlled flow of 200 cc/min argon purge was used during pyrolysis. The system was purged for at least 6 h prior to pyrolysis in order to drive out all the air present in the system. Prior to start of the pyrolysis, the oxygen analyzer displayed an initial oxygen concentration of ~0.5 ± 0.1 ppm oxygen in the pyrolysis quartz tube. A needle valve was used to control the flow rate of argon, with the flow rate monitored before and after the pyrolysis run using a universal gas flow-meter (Agilent Technologies, ADM 1000). The CMS dense films obtained were tested for pure gas C_2H_4 and C_2H_6 permeation at 35 °C and 50 psia feed pressure. As seen from Fig. 6, inert gas pyrolysis yielded results comparable to vacuum pyrolysis with a slightly higher permeability and lower selectivity, indicating feasibility for scale-up.

Kiyono et al. [43] reported an "oxygen-doping" method using controlled concentrations of oxygen in the pyrolysis purge stream, where in the oxygen tends to chemisorb selectively at the ultramicropores (ultramicropore defects are believed to be ~17 times more reactive than the basal plane [49]), thus allowing a means to tune the CO_2/CH_4 separation performance. For CMS films derived by pyrolyzing Matrimid® at 550 °C, they reported a decrease in both CO_2 permeability and CO_2/CH_4 selectivity (from the vacuum pyrolysis performance) with increase in oxygen concentration from 3 to 100 ppm in argon. At a lower pyrolysis temperature of 500 °C, an increase of oxygen concentration from 1 to 30 ppm showed an increase in selectivity with a corresponding decrease in permeability, but the performance was similar to the 550 °C vacuum pyrolysis. The results reported by Kiyono et al. [43] indicate that the use of "oxygen-doping" to tune the C_2H_4/C_2H_6 separation performance of CMS fabricated from Matrimid® may require significant modification for the larger C_2H_4/C_2H_6 pair with relatively smaller size difference between the two gas molecules. This will be a topic of future study.

Table 2 – % Mass loss during vacuum pyrolysis for the 675 °C Protocol and 675 °C_Fast protocol. The data is averaged over two runs for each protocol with three samples in each run. The % residual mass for the 675 °C protocol and 675 °C_Fast protocol compare well with the respective TGA data shown above.

Vacuum pyrolysis	675 °C protocol	675 °C_Fast protocol
% Mass loss	40.12	41.83
% Residual mass	59.88	58.17

4.6. *Ethylene/ethane mixed gas permeation*

Mixed gas permeation tests were performed at 35 °C on Matrimid® 550 °C-CMS and 675 °C_Fast-CMS pyrolyzed under vacuum. The feed composition used was 63.2 mol% C_2H_4 and 36.8 mol% $C_2H_6$with a total feed pressure of 50 psia and the stage cut was maintained at <1%. The mixed gas feed composition used here for lab-scale testing is similar to the feed composition currently employed for some industrial scale distillation columns. The steady state permeation results are summarized in Table 3.

It is seen that there is a decrease in permeability and a slight increase in selectivity compared to pure gas measurements, and these seem to be due to the complicated competition effects between the very similar C_2H_4 and C_2H_6 molecules. It may be that the double-bonded C_2H_4 can interact more strongly with the sp^2 hybridized CMS basal plane, favoring C_2H_4 sorption and possibly hindering C_2H_6, with a resultant small increase in mixed gas selectivity. The competition between C_2H_4 and C_2H_6 however does hinder diffusion of both the gases, with a resultant lower permeability in the case of mixed gas. This fact notwithstanding, as seen from Table 3, pure gas measurements give a good estimate of the CMS performance expected using mixed gas compositions representative of real industrial feeds. Sorption experiments will be pursued in the future in order facilitate further understanding of the competition between C_2H_4 and C_2H_6, and will also be useful in predicting mixed gas permeability and selectivity from pure gas properties using Langmuir sorption parameter (Eq. (4)).

4.7. *Effect of permeation temperature on ethylene/ethane separation performance*

The effect of permeation temperature was studied at two pyrolysis temperatures. For preliminary investigation, pure C_2H_4 and C_2H_6 permeation tests were done at 35 and 50 °C using 50 psia feed pressure, on a Matrimid® film pyrolyzed under vacuum at 550 °C using Protocol 1. Apparent diffusion and sorption data were calculated from the permeability values using the time-lag method described above. The diffusion selectivity at 35 °C and 50 °C are 4.5 and 4.8, respectively while the sorption selectivity lies in the range of 1.3–1.4, indicating that CMS selectivity comes mostly from its diffusion selectivity while the sorption selectivity contribution is similar to polymeric membranes. Using Arrhenius-type relationships (Eqs. (6) and (7)), it was further seen that the activation energies for permeation and diffusion through the 550 °C-CMS for C_2H_4 and C_2H_6 are similar (Table 4), presumably because of their similar size and properties. In addition, as suggested, the major contribution to diffusion selectivity comes from its 'entropic selectivity' while the 'energetic selectivity' is low. This entropic selectivity is essentially a measure of the configurational advantage that the 'slimmer' C_2H_4 molecule has over C_2H_6 in transport through the 'slit-like' CMS structure. In other words, an entropic selectivity of 14.7 (Table 4) indicates that C_2H_4 is 14.7 times more likely to orient itself in a configuration that allows it to diffuse though the CMS pores compared to C_2H_6. Since polymers do not possess a rigid structure as in the case of CMS, they do not allow taking advantage of this configurational orientation, and this is the main reason why CMS membranes can deliver attractive C_2H_4/C_2H_6 separation performance [34].

Since this preliminary study was carried out using only two permeation temperatures with the results assumed to fit the Arrhenius-type equations, a more detailed investigation was done for the vacuum pyrolyzed 675 °C-Fast Carbon which gave optimum C_2H_4/C_2H_6 performance. Pure C_2H_4 and C_2H_6 permeation, using 50 psia feed pressure, was done at three temperatures: 30, 35 and 45 °C. Limitations on the transducers and epoxy used in the study did not allow for measurements at higher temperatures. The Arrhenius-type plots for permeability and diffusivity are shown in Fig. 12 and the results are tabulated in Table 3. The data used are average values from two tests each with <10% standard deviation in permeabilities. As noted in the case of the 550 °C-CMS, C_2H_4 and C_2H_6 show similar activation energies for both permeation and diffusion for the 675 °C_Fast-CMS as well. The activation energies for both permeation and diffusion are higher for the 675 °C_Fast carbon than for the 550 °C-CMS, representing greater resistance to transport in the former. However, the pre-exponential factors for permeation and diffusion increase several orders of magnitude in going from the 550 °C-CMS to the 675 °C_Fast-CMS, thus resulting in an overall increase in both permeability and diffusivity for the 675 °C_Fast-CMS. An increase in pre-exponential factor for diffusion can result from either an increase in activation entropy of diffusion or diffusive jump length (Eq. (12)) or a combination of the two [37]. Since it is hard to imagine significant increase in jump lengths in going from 550 to 675 °C, increase in pre-exponential factor for the 675 °C_Fast-CMS is likely a result of increase in the activation entropy of diffusion. The sorption selectivity for the 675 °C_Fast-CMS is similar to 550 °C-CMS while the diffusion selectivity is higher for the former, thus resulting in an increase in selectivity. As before, while the energetic contribution to the diffusion selectivity remains low, an exceptionally high entropic selectivity of 16.2 for the 675 °C_Fast-CMS indicates a further configurational advantage for C_2H_4 over C_2H_6.

Singh and Koros [34] carried out similar entropic and energetic selectivity calculations for the O_2/N_2 gas pair for transport in CMS. It is worth noting that while Singh and Koros [37] observed significant energetic contribution to overall diffusion selectivity for O_2/N_2 separation, such effect is not observed here because of the similar activation energies of C_2H_4 and C_2H_6. This also leads to the fact that with a small increase in permeation temperature there is no loss in selectivity (see Table 4) for C_2H_4/C_2H_6 separation as is observed in the case of most gas separations. Singh and Koros [34] evaluated the theoretical limits for entropic selectivity, essentially equal to the ratio of the partition functions in the transition state to

Table 3 – Pure and mixed gas (63.2% C_2H_4/ 36.8% C_2H_6) permeation results at 35 °C and 50 psia total feed pressure.

State	Total feed pressure (psia)	Pure gas		Mixed gas	
		$P_{C_2H_4}$ (Barrer)	$\alpha_{C_2H_4/C_2H_6}$	$P_{C_2H_4}$ (Barrer)	$\alpha_{C_2H_4/C_2H_6}$
550 °C-CMS, vacuum	50	14.5 ± 1.35	6.6 ± 0.26	8.3	7.7
675 °C_Fast-CMS, vacuum	50	16.7	11.7	10.9	12.3

Table 4 – Effect of permeation temperature on C_2H_4/C_2H_6 separation for 550 °C-CMS and 675 °C_Fast-CMS.

	550 °C-CMS		675 °C_Fast-CMS	
P_A/P_B	30 °C		12.1	
	35 °C	6.3	35 °C	11.7
	50 °C	6.3	45 °C	12.1
D_A/D_B	30 °C		8.1	
	35 °C	4.5	35 °C	8.3
	50 °C	4.8	45 °C	8.4
$\mathbb{S}_A/\mathbb{S}_B$	30 °C		1.5	
	35 °C	1.4	35 °C	1.4
	50 °C	1.3	45 °C	1.4
E_{PA} (kcal/mol)	7.1		12.2	
E_{PB} (kcal/mol)	7.2		12	
P_{Ao} (Barrer)	1.60E+06		6.20E+09	
P_{Bo} (Barrer)	3.00E+05		4.20E+08	
E_{DA} (kcal/mol)	10.4		17.6	
E_{DB} (kcal/mol)	9.7		17.1	
D_{Ao} (cm^2/s)	1.90E−02		3.60E+03	
D_{Bo} (cm^2/s)	1.30E−03		2.20E+02	
Entropic contribution	14.7		16.2	
Energetic contribution	~0.3		~0.5	

the normal state of the two components $\left[\frac{(F^{\neq}/F)_A}{(F^{\neq}/F)_B}\right]$, for the O_2/N_2 gas pair in transport through a slit-like CMS pore by taking into account the degrees of freedom for the two molecules in the normal (sorbed) and transition state. O_2 molecule can pass through the CMS slit-shaped pores rotating about either axis of rotation. N_2, on the other hand, may pass through rotating only about one axis as shown in Fig. 13a. Both O_2 and N_2 can translate along the graphitic planes, transverse to the direction of diffusion. Depending on whether or not an additional vibrational degree of freedom is present for N_2, in lieu of the lost rotational degree of freedom, in the activated state, the entropic selectivity calculated is 3.7–9.0 (see [34] for detailed calculation). These values encompass the experimentally observed O_2/N_2 entropic selectivity range of 4.9–8.8 for CMS [34,50]. A similar analogy can be extended to the C_2H_4/C_2H_6 case as shown in Fig. 13b. However, compared to the simple O_2/N_2 case where a molecule can either pass

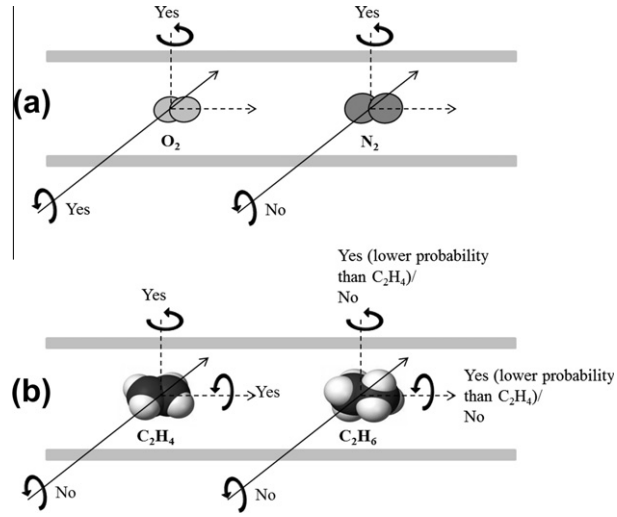

Fig. 13 – View of a CMS slit-shaped pore in the direction of diffusion with illustration of the rotational degrees of freedom in the activated state. (a) O_2/N_2 system: O_2 can pass through rotating about both axes while N_2 can rotate only about one axis. (b) C_2H_4/C_2H_6 system: C_2H_4 can pass through rotating about two axes with greater probability than C_2H_6. C_2H_6 may either get rejected completely at all configurations or may pass through rotating about either one axis or two axes but with a smaller probability than C_2H_4.

through or get rejected, the entropic selectivity for the more complex C_2H_4 and C_2H_6 molecules is much more complicated to predict. For these more complex molecules, the entropic selection would now be dependent on the probability of many subtle configurational differences enabling a particular molecule to get through the diffusion-limiting ultramicropore. As shown in Fig. 13b, at a particular configuration, the 'skinnier' C_2H_4 will pass through the 'slit-shaped' CMS pore with greater ease (probability) while C_2H_6 will require greater effort (continuous rotation about an axis) if at all it can pass through in the same configuration. Computing the theoretical limits for C_2H_4/C_2H_6 entropic selectivity is thus not simple, as for

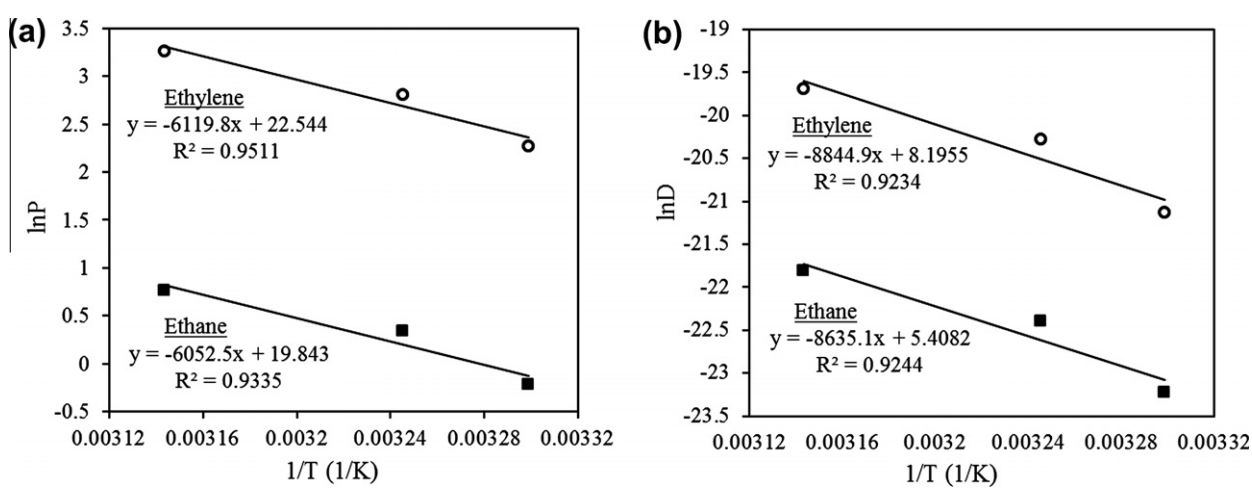

Fig. 12 – Arrhenius-type plots for (a) permeability (Eq. (6)) and (b) diffusivity (Eq. (7)) for C_2H_4/C_2H_6 separation using 675 °C_Fast-CMS. The data represents average values from two tests each with <10% standard deviation in permeabilities.

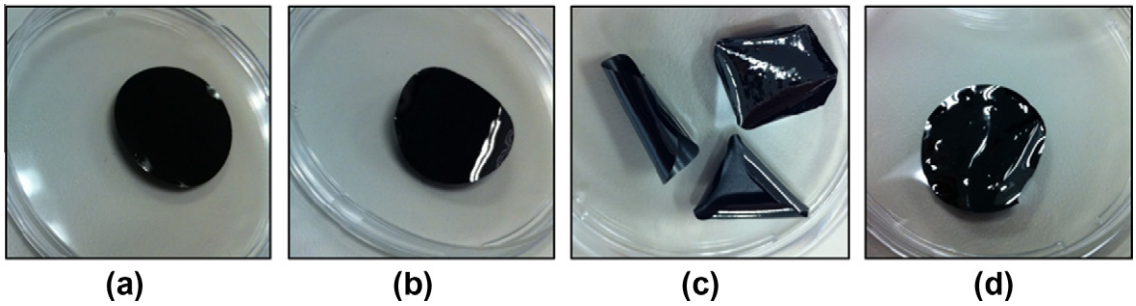

Fig. 14 – Different types of CMS films formed as a result of pyrolysis (a) flat film, (b) slightly curled film, (c) over-curled film, and (d) crinkled film.

the case of O_2/N_2, and would require extensive modeling. Besides, unlike O_2/N_2, the parameters involved in such a theoretical calculation (see [34]) are not available for C_2H_4/C_2H_6. Detailed modeling being beyond the scope of this study has thus not being pursued in detail here; however, we may consider this in the future.

4.8. *Production of "testable" CMS dense films from Matrimid®*

Production of "testable" (suitable for permeation measurements) CMS dense films from Matrimid® can be challenging. Since CMS films are brittle compared to polymer films, it is important to get CMS films that can be handled and masked appropriately for permeation measurements (see Section 3.3 for details). Several factors have been identified as being responsible in the formation of testable CMS dense films. Before discussing these factors, it is useful to describe the various different types of films that can result from pyrolyzing Matrimid® precursor films. For convenience, the resultant CMS films can be categorized into four types (Fig. 14): (a) flat films (testable), (b) slightly curled (bent) films (testable), (c) over-curled films (not testable) and (d) crinkled (wavy) films (not testable).

Flat films can easily be masked for permeation. Slightly curled films generally resulted from pyrolysis under inert gas argon atmosphere. Such films are flexible and can be masked for permeation with a >95% success rate. Over-curled films and crinkled films are impossible to mask and break invariably. The detailed cause in terms of pyrolysis condition for these different types of films is not yet well understood, but with experience the first two types (a and b) can be created and tested relatively easily.

A primary reason for production of crinkled or over-curled films is believed to be stress present on the precursor films prior to pyrolysis, which can result due to several factors. The casting technique for precursor films is extremely important. A Teflon disc is preferred as the casting substrate for solution casting of Matrimid® precursor films, as opposed to so-called "ring casting" on a glass surface using a metal ring. Casting on a Teflon disc minimized inherent stress on the resulting precursor film by preventing adhesion of the final vitrified polymer films to the surface of the substrate. In addition, it is important to maintain a very slow evaporation rate during the casting process to minimize resultant stress on the precursor films due to vitrification. Precursor films cast on Teflon resulted in >90% success rate in formation of testable CMS dense films while ring-casting on a glass surface resulted in crinkled or over-curled films in most cases. It was also found that using thicker precursor dense films resulted in less curling of films due to pyrolysis. Lastly, cutting of precursor films into small circles for pyrolysis can also result in stresses. In order to avoid this, films were cut using a sharp die-cutter by hitting uniformly with one single blow of a hammer. This results in distribution of the stress on the unwanted area around the desired circle. On some occasions, scissors were used to detach the circular film at points that were not cut using the die-cutter. In addition to the precautions practiced in precursor film preparation, experiments were conducted to remove residual stresses on the precursor films prior to pyrolysis by soaking the polymer films just below as well as at the glass transition temperature (310 °C) of Matrimid® for 2 h. This however did not significantly affect the resultant CMS dense films.

The nature of the support used for pyrolysis is also important. Pyrolysis over a wire mesh support results in CMS films bearing impressions of the wire mesh with stress points at which they tend to crack easily. A solid quartz support results in over-curled films because of hindered transfer of the pyrolysis by-products. A ribbed or channeled quartz plate on the other hand allows for free diffusion of the pyrolysis by-products thus resulting in testable CMS film formation. This study thus uses a channeled quartz plate for the production of CMS dense films for C_2H_4/C_2H_6 separation. Recently it has also been found that use of the same quartz support and quartz tube over an extended period of time eventually tends to create crinkled CMS films. The reason for this is however not yet well understood by the authors. After repeated burn out in air, the ribbed quartz plate and quartz tube eventually show signs of erosion with a somewhat roughened surface, and this presumably causes the odd crinkling effect.

5. Conclusions

CMS dense films were successfully fabricated from commercial polyimide Matrimid® for C_2H_4/C_2H_6 separation. The CMS films showed significant improvement in separation performance over their precursor under a wide range of pyrolysis conditions and performance was seen to surpass the estimated C_2H_4/C_2H_6 polymeric upper bound line. With increase in pyrolysis temperature, C_2H_4 permeability was found to increase with a corresponding decrease in C_2H_4/C_2H_6 selectivity up to an optimum temperature, beyond which permeability dropped drasti-

cally with no significant increase in the selectivity. Optimum separation performance was obtained in the range of 650–675 °C with a C_2H_4 permeability of 14–15 Barrer and a high C_2H_4/C_2H_6 selectivity of ~12.These combined properties are well beyond those of the precursor material and the estimated polymer 'upper bound'. C_2H_4 diffusion and C_2H_4/C_2H_6 diffusion selectivity were shown to follow a similar trend as permeability and overall selectivity. These changes have be explained qualitatively by considering changes in the hypothetical ultramicropore distribution indicative of the critical molecular sieving selective pores of the CMS membranes. A modified heating protocol with a final pyrolysis temperature of 675 °C further improved the separation performance. In addition, CMS films produced by pyrolysis under an inert argon atmosphere showed results comparable to vacuum pyrolysis, indicating feasibility of scale-up. Mixed gas permeation experiments, using a 63.2 mol% C_2H_4–36.8 mol% C_2H_6 mixture, showed a slightly lower C_2H_4 permeability with an increase in C_2H_4/C_2H_6 selectivity rather than a decrease which is often seen with polymers. Nevertheless, pure gas measurements can give a reasonably good estimate of the CMS performance expected using mixed gas compositions representative of real industrial feeds. Further sorption experiments will be pursued in the future in order facilitate complete understanding of the complicated competition effects between C_2H_4 and C_2H_6, and for predicting mixed gas permeability and selectivity from pure gas properties. Lastly, the dependence on permeation temperature was evaluated for the CMS dense films, indicating an increase in C_2H_4 permeability with no significant change in C_2H_4/C_2H_6 selectivity. The activation energies for both permeation and diffusion for C_2H_4 and C_2H_6 were found to be very similar. Further, the C_2H_4/C_2H_6 selectivity of CMS membranes was found to come mainly from its diffusion selectivity, whereas the sorption selectivity was similar to polymeric membranes. In addition, the CMS membranes showed a very high 'entropic selectivity', indicating strong dependence on the probability of many subtle configurational differences enabling the 'slimmer' C_2H_4 molecule to preferably get through the rigid 'slit-shaped' diffusion-limiting CMS ultramicropores. This seems to be the main reason why CMS membranes can deliver attractive C_2H_4/C_2H_6 separation performance.

Acknowledgements

The authors thank The Dow Chemical Company for funding this work. The authors especially thank Mark Brayden, Marcos Martinez and Duncan Coffey for helpful discussions and comments regarding this work. The authors also acknowledge additional support provided by King Abdullah University of Science and Technology (KAUST).

REFERENCES

[1] True WR. OGJ focus global ethylene production continues advance in 2009. Oil Gas J 2010;108(27):34–8.
[2] Wu ZB, Han SS, Cho SH, Kim JN, Chue KT, Yang RT. Modification of resin-type adsorbents for ethane/ethylene separation. Ind Eng Chem Res 1997;36(7):2749–56.
[3] Caballero JA, Grossmann IE, Keyvani M, Lenz ES. Design of hybrid distillation–vapor membrane separation systems. Ind Eng Chem Res 2009;48(20):9151–62.
[4] Gottschlich DE, Roberts DL. Energy minimization of separation processes using conventional/membrane hybrid systems. US Department of Energy USA, DE91 004710; 1990.
[5] Merkel T, Blanc R, Zeid J, Suwarlim A, Firat B, Wijmans S, et al. Separation of olefin/paraffin mixtures with carrier facilitated membranes. US Department of Energy USA, DE-FC36-04GO14151; 2007.
[6] Koros WJ. Evolving beyond the thermal age of separation processes: membranes can lead the way. AIChE J 2004;50(10):2326–34.
[7] Robeson LM. Correlation of separation factor versus permeability for polymeric membranes. J Membr Sci 1991;62(2):165–85.
[8] Robeson LM. The upper bound revisited. J Membr Sci 2008;320(1–2):390–400.
[9] Burns RL, Koros WJ. Defining the challenges for C_3H_6/C_3H_8 separation using polymeric membranes. J Membr Sci 2003;211(2):299–309.
[10] Chan SS, Chung TS, Liu Y, Wang R. Gas and hydrocarbon (C2 and C3) transport properties of co-polyimides synthesized from 6FDA and 1,5-NDA (naphthalene)/Durene diamines. J Membr Sci 2003;218(1–2):235–45.
[11] Chan SS, Wang R, Chung TS, Liu Y. C-2 and C-3 hydrocarbon separations in poly(1,5-naphthalene-2,2′-bis(3,4-phthalic)hexafluoropropane)diimide (6FDA-1,5-NDA) dense membranes. J Membr Sci 2002;210(1):55–64.
[12] Tanaka K, Taguchi A, Hao J, Kita H, Okamoto K. Permeation and separation properties of polyimide membranes to olefins and paraffins. J Membr Sci 1996;121(2):197–207.
[13] Staudt-Bickel C, Koros WJ. Olefin/paraffin gas separations with 6FDA-based polyimide membranes. J Membr Sci 2000;170(2):205–14.
[14] Pinnau I, Toy LG. Solid polymer electrolyte composite membranes for olefin/paraffin separation. J Membr Sci 2001;184(1):39–48.
[15] Teramoto M, Shimizu S, Matsuyama H, Matsumiya N. Ethylene/ethane separation and concentration by hollow fiber facilitated transport membrane module with permeation of silver nitrate solution. Sep Purif Technol 2005;44(1):19–29.
[16] Teramoto M, Takeuchi N, Maki T, Matsuyama H. Ethylene/ethane separation by facilitated transport membrane accompanied by permeation of aqueous silver nitrate solution. Sep Purif Technol 2002;28(2):117–24.
[17] Marsh H. Introduction to carbon science. England: Butterworth; 1989. p. 2–11.
[18] Steel KM. Carbon membranes for challenging gas separations. Austin TX USA, The University of Texas at Austin, Ph.D. thesis; 2000.
[19] Kiyono M, Williams PJ, Koros WJ. Effect of pyrolysis atmosphere on separation performance of carbon molecular sieve membranes. J Membr Sci 2010;359(1–2):2–10.
[20] Barsema JN, Klijnstra SD, Balster JH, van der Vegt NFA, Koops GH, Wessling M. Intermediate polymer to carbon gas separation membranes based on Matrimid PI. J Membr Sci 2004;238(1–2):93–102.
[21] Saufi SM, Ismail AF. Fabrication of carbon membranes for gas separation – a review. Carbon 2004;42(2):241–59.
[22] Koresh JE, Sofer A. Molecular-sieve carbon permselective membrane. 1. Presentation of a new device for gas-mixture separation. Sep Sci Technol 1983;18(8):723–34.
[23] Williams PJ. Analysis of factors influencing the performance of CMS membranes for gas separation. Atlanta GA USA, Georgia Institute of Technology, Ph.D. thesis; 2006.

[24] Singh A. Membrane materials with enhanced selectivity: an entropic interpretation. Austin TX USA, The University of Texas at Austin, Ph.D. thesis; 1997.
[25] Vu DQ, Koros WJ, Miller SJ. High pressure CO_2/CH_4 separation using carbon molecular sieve hollow fiber membranes. Ind Eng Chem Res 2002;41(3):367–80.
[26] Qiu W, Chen CC, Xu L, Cui L, Paul DR, Koros WJ. Sub-T(g) cross-linking of a polyimide membrane for enhanced CO(2) plasticization resistance for natural gas separation. Macromolecules 2011;44(15):6046–56.
[27] Das M, Koros WJ. Performance of 6FDA–6FpDA polyimide for propylene/propane separations. J Membr Sci 2010;365(1–2):399–408.
[28] Hayashi J, Mizuta H, Yamamoto M, Kusakabe K, Morooka S, Suh SH. Separation of ethane/ethylene and propane/propylene systems with a carbonized BPDA-pp′ODA polyimide membrane. Ind Eng Chem Res 1996;35(11):4176–81.
[29] Okamoto K, Kawamura S, Yoshino M, Kita H, Hirayama Y, Tanihara N, et al. Olefin/paraffin separation through carbonized membranes derived from an asymmetric polyimide hollow fiber membrane. Ind Eng Chem Res 1999;38(11):4424–32.
[30] Fuertes AB, Menendez I. Separation of hydrocarbon gas mixtures using phenolic resin-based carbon membranes. Sep Purif Technol 2002;28(1):29–41.
[31] Xu L, Rungta M, Koros WJ. Matrimid® derived carbon molecular sieve hollow fiber membranes for ethylene/ethane separation. J Membr Sci 2011;380(1–2):138–47.
[32] Jenkins GM, Kawamura K. Polymeric carbons – carbon fiber, glass and char. London: Cambridge University Press; 1976. p. 52–82 [Chapter 4].
[33] Pierson HO. Handbook of carbon, graphite, diamond, and fullerenes. New Jersey: Noyes; 1993. p. 43–51.
[34] Singh A, Koros WJ. Significance of entropic selectivity for advanced gas separation membranes. Ind Eng Chem Res 1996;35(4):1231–4.
[35] Singh-Ghosal A, Koros WJ. Energetic and entropic contributions to mobility selectivity in glassy polymers for gas separation membranes. Ind Eng Chem Res 1999;38(10):3647–54.
[36] Crank J, Park GA. Diffusion in polymers. New York: Academic Press; 1968. p. 41–72 [Chapter 2].
[37] Singh-Ghosal A, Koros WJ. Air separation properties of flat sheet homogeneous pyrolytic carbon membranes. J Membr Sci 2000;174(2):177–88.
[38] Glasstone S, Laidler KJ, Eyring H. The theory of rate processes. 1st ed. New York: McGraw-Hill Book; 1941. p. 524–5.
[39] Steel KM, Koros WJ. Investigation of porosity of carbon materials and related effects on gas separation properties. Carbon 2003;41(2):253–66.
[40] Steel KM, Koros WJ. An investigation of the effects of pyrolysis parameters on gas separation properties of carbon materials. Carbon 2005;43(9):1843–56.
[41] Suda H, Haraya K. Gas permeation through micropores of carbon molecular sieve membranes derived from Kapton polyimide. J Phys Chem B 1997;101(20):3988–94.
[42] Geiszler VC, Koros WJ. Effects of polyimide pyrolysis conditions on carbon molecular sieve membrane properties. Ind Eng Chem Res 1996;35(9):2999–3003.
[43] Kiyono M, Williams PJ, Koros WJ. Effect of polymer precursors on carbon molecular sieve structure and separation performance properties. Carbon 2010;48(15):4432–41.
[44] Oyama TS, Stagg-Williams SM. Inorganic polymeric and composite membranes – structure, function and other correlations. Elsevier; 2010. p. 137–73 [Chapter 7].
[45] Pye DG, Hoehn HH, Panar M. Measurement of gas permeability of polymers. I: permeabilities in constant volume/variable pressure apparatus. J Appl Polym Sci 1976;20(7):1921–31.
[46] Pye DG, Hoehn HH, Panar M. Measurement of gas permeability of polymers. II: apparatus for determination of permeabilities of mixed gases and vapors. J Appl Polym Sci 1976;20(2):287–301.
[47] Ilinitch OM, Semin GL, Chertova MV, Zamaraev KI. Novel polymeric membranes for separation of hydrocarbons. J Membr Sci 1992;66(1):1–8.
[48] Ilinich OM, Zamaraev KI. Separation of ethylene and ethane over polyphenyleneoxides membranes: transient increase of selectivity. J Membr Sci 1993;82(1–2):149–55.
[49] Grisdale RO. The properties of carbon contacts. J Appl Phys 1953;24(10):1288–96.
[50] Karger J, Ruthven DM. Diffusion in zeolites and other microporous solids. New York: Wiley Interscience; 1992. p. 414–21.